

In the format provided by the authors and unedited.

## Sequential bottom-up assembly of mechanically stabilized synthetic cells by microfluidics

Marian Weiss,<sup>1,2‡</sup> Johannes Patrick Frohnmayer,<sup>1,2‡</sup> Lucia Theresa Benk,<sup>1,2‡</sup> Barbara Haller,<sup>1,2</sup> Jan-Willi Janiesch,<sup>1,2</sup> Thomas Heitkamp,<sup>3</sup> Michael Börsch,<sup>3</sup> Rafael B. Lira,<sup>4</sup> Rumiana Dimova,<sup>4</sup> Reinhard Lipowsky,<sup>4</sup> Eberhard Bodenschatz,<sup>5</sup> Jean-Christophe Baret,<sup>6,7</sup> Tanja Vidakovic-Koch,<sup>8</sup> Kai Sundmacher,<sup>8,9</sup> Ilia Platzman,<sup>1,2\*</sup> and Joachim P. Spatz<sup>1,2\*</sup>

<sup>1</sup>Department of Cellular Biophysics, Max Planck Institute for Medical Research, Jahnstraße 29, 69120 Heidelberg, Germany

<sup>2</sup>Department of Biophysical Chemistry, University of Heidelberg, Im Neuenheimer Feld 253, 69120 Heidelberg, Germany

<sup>3</sup>Single-Molecule Microscopy Group, Jena University Hospital, Friedrich Schiller University Jena, 07743 Jena, Germany

<sup>4</sup>Theory & Bio-Systems, Max Planck Institute of Colloids and Interfaces, 14424 Potsdam, Germany

<sup>5</sup>Laboratory for Fluid Dynamics, Pattern Formation and Biocomplexity, Max Planck Institute for Dynamics and Self-Organization, 37077 Göttingen, Germany

<sup>6</sup>Droplets, Membranes and Interfaces, Max Planck Institute for Dynamics and Self-Organization, 37077 Göttingen, Germany

<sup>7</sup>Soft Micro Systems, CNRS, Univ. Bordeaux, CRPP, UPR 8641, 115 Avenue Schweitzer, 33600 Pessac, France

<sup>8</sup>Process System Engineering, Max Planck Institute for Dynamics of Complex Technical Systems, 39106 Magdeburg, Germany

<sup>9</sup>Otto-von-Guericke University Magdeburg, Process Systems Engineering, Universitätsplatz 2, 39106 Magdeburg, Germany

Corresponding authors:

[ilia.platzman@mpimf-heidelberg.mpg.de](mailto:ilia.platzman@mpimf-heidelberg.mpg.de) and [joachim.spatz@mpimf-heidelberg.mpg.de](mailto:joachim.spatz@mpimf-heidelberg.mpg.de)

## Supplementary Text

### Supplementary Movie Legends

#### Supplementary Movie 1

The formation of a dsGUV out of the encapsulated GUVs.

Representative time-lapse fluorescence microscopy of the process showing the transformation of the encapsulated GUVs (ATTO 488-labeled DOPE) into a continuous supported lipid bilayer at the droplet inner interface. To transform the encapsulated GUVs into a supported lipid bilayer at the copolymer-stabilized droplet inner interface, 10 mM  $Mg^{2+}$  was applied during droplet production or by means of pico-injection.

#### Supplementary Movie 2

Microfluidic release device.

The video shows the dsGUVs encounter the aqueous phase in a wide perpendicular channel. To minimize the mechanical impact on the dsGUVs at the oil/water junction, the droplets were decelerated using passive trapping structures within the microfluidic channels (i.e., rows of pillars separated by distances smaller than the representative droplets dimensions), which we designed for the efficient release of GUVs.

#### Supplementary Movie 3

Pyranine as a pH sensor inside microfluidic droplets.

The video shows water-in-oil droplets immobilized in a microfluidic trapping device. The pH-sensitive fluorophore pyranine (concentration: 50  $\mu$ M) in ATP activity buffer was encapsulated into the droplets. To change the pH inside the droplets via the oil phase, acidic oil (containing 1  $\mu$ L of trifluoroacetic acid per 1 ml FC40 oil) and basic oil (containing 1  $\mu$ L of propyl amine per 1 ml FC40 oil) were alternately flushed through the device. As a result, the pH inside the droplets changed accordingly from acidic to basic and vice versa. The encapsulated fluorophore pyranine was simultaneously excited at 405nm and 458nm wavelength and the corresponding emission signal was recorded. Dominant 405nm detection signal indicated by blue color corresponds to basic pH, dominant 458nm detection signal indicated by green color corresponds to acidic pH.

## Supplementary Methods

### Preparation of large unilamellar vesicles (LUVs) and free-standing giant unilamellar vesicles (GUVs).

Lipids used in this study: 1,2-dioleoyl-sn-glycero-3-phosphocholine (DOPC), 1,2-dioleoyl-sn-glycero-3-phosphoethanolamine (DOPE), 1,2-dioleoyl-sn-glycero-3-phospho-L-serine (DOPS), 1,2-dioleoyl-sn-glycero-3-[(N-(5-amino-1-carboxypentyl)iminodiacetic acid) succinyl] (DGS-NTA), 1,2-dioleoyl-sn-glycero-3-phosphoethanolamine-N-(lissamine rhodamine B sulfonyl) (RhB DOPE), 1-palmitoyl-2-hydroxy-sn-glycero-3-phosphate (Phosphatidic acid), L- $\alpha$ -phosphatidylcholine (Egg PC), L- $\alpha$ -phosphatidylglycerol (Egg PG) were purchased from Avanti (Avanti Polar Lipids, USA) and used without further purification. ATTO 488 1,2-dioleoyl-sn-glycero-3-phosphoethanolamine was purchased from ATTO TEC (Siegen, Germany);

To obtain the formation of dsGUVs, solutions of LUVs or GUVs, consisting of different lipid compositions, were generated according to previously reported protocols.<sup>1, 2</sup> In brief, lipids were dissolved in pure chloroform, mixed at desired composition and concentration and dried

under a gentle stream of nitrogen. To remove traces of the solvent, lipids were kept under vacuum in desiccator for roughly 1 h. Dried lipids were then resuspended by addition of the desired buffer, followed by one hour of vortexing. LUV size was homogenized by extruding the solution 7 times through a polycarbonate filter (Whatman, Germany) with a pore size of 50 nm using an extruder (Avanti Polar Lipids, USA). The mean LUV diameter distribution was determined to be  $100 \pm 10$  nm using DLS. Solutions containing LUVs were stored at 4°C for not longer than 48 h or used immediately after production.

GUVs consisting of DOPC:DOPE:DOPS 8:1:1, including 1% ATTO 488-labeled DOPE were formed using the electroformation protocols as described previously.<sup>2</sup> In brief, lipid mixtures at the desired concentration (from 1 to 5 mM) were dissolved in pure chloroform and spread onto two indium tin oxide (ITO) coated glasses (Sigma-Aldrich, Germany). Following chloroform evaporation, the electroformation cell was assembled. Towards this end, the two ITO coated glasses were faced to each other with the conductive sides. To avoid direct contact two Teflon spacers (1 mm) were used. Copper tape (3M, USA) was used to connect the conducting sides with a signal generator (RS Components, Germany). Subsequently, the chamber was filled with Milli-Q water (Millipore filtered) and sealed with two-component glue (Twinsil Picodent GmbH, Germany). An alternating electrical potential of 10 Hz at 1 V amplitude was applied for 2 h to form GUVs. Finally the GUVs were collected using a syringe. Following vesicles production, the solutions were used immediately for encapsulation into microfluidic water-in-oil copolymer-stabilized droplets.

**Block copolymer surfactant synthesis.** Three types of block-copolymer surfactants were synthesized according to protocols reported earlier<sup>3, 4</sup> and used to produce droplets: Two triblock-copolymers PFPE(7000 g/mol)-PEG(1400 g/mol)-PFPE(7000 g/mol) (TRI7000) and PFPE(2500 g/mol)-PEG(600 g/mol)-PFPE(2500 g/mol) (TRI2500) and a gold-linked diblock-copolymer surfactant Au-PEG(436 g/mol)-PFPE(7000 g/mol). Following synthesis, triblock surfactants were mixed separately with gold-linked surfactants and dissolved in FC-40 fluorinated oil (3M, USA) to the final concentrations of 2.5 mM and 3  $\mu$ M for triblock and gold-linked surfactants, respectively. NOTE: The two types of triblock copolymer surfactants (i.e. TRI7000 and TRI2500) mixed with gold-linked surfactants were tested and compared in all experiments. If not stated otherwise, the same results were observed.

**Droplet-based microfluidics.** Droplet-based microfluidic devices made of PDMS (Sylgard 184, Dow Corning, USA) were prepared by photo- and soft-lithography methods<sup>5, 6</sup> as described previously.<sup>3</sup> To control the droplet diameter during their creation, two different nozzle designs at the flow-focusing junction were implemented (Supplementary Figures 4 A and B). Syringe pumps PUMP 11 ELITE (Harvard apparatus, USA) were used to control flow rates of 120  $\mu$ L/h for the aqueous phase and 160  $\mu$ L/h for the oil phase as required for stable droplet creation (diameter  $d = 40$   $\mu$ m) at the rate of 1 kHz. In case of big droplets ( $d = 100$   $\mu$ m) the flow rates were adjusted to 650 and 850  $\mu$ L/h for aqueous and oil phases, respectively to achieve a stable droplet creation at a rate of 1 kHz.

Due to the variety of required cellular components in the droplets the microfluidic device was integrated with small and compact electrodes to apply an electric potential. Electrical fields allow destabilization (poration) of surfactants and lipid bilayers towards controlled injection (pico-injection) of different cellular components into the droplets. The design of the droplet-based pico-injection unit was adapted from Abate et al.<sup>7</sup> Droplets were introduced into the device using a MFCS-EZ flow control system (Fluigent, France). The spacing between the droplets was controlled through addition of oil via the second oil channel (Supplementary Figure 4F). Following separation step, isolated droplets passed an alternating electrical field (frequency 1kHz, potential 250 V) generated by HM 8150 signal generator (HAMEG, Germany) and amplified by 623B-H-CE amplifier (TREK, USA) and two electrodes made of

Indalloy 19 (51% indium, 32.5% bismuth, 16.5% tin, GPS Technologies, Germany). This process destabilizes the droplet copolymer shell and lipid bilayer and allows introduction of bio-reagents via a pressurized injection channel (Supplementary Figure 4G). The injection volume can be ranged between 1 to 100  $\mu\text{l}$ , dependent on the applied pressure.

For analysis, droplets were collected and transferred to the observation chamber (Supplementary Figure 5). The chamber was made of two single or sandwiched stripes of double face sticky tapes (Tesa, Germany. Thickness  $\approx 80 \mu\text{m}$  or  $160 \mu\text{m}$  for analysis of small and large droplets, respectively) as spacers, glued between two cover slips (Carl Roth, Germany). Finally, the chamber was filled with surfactant-containing oil and closed by two-component glue (Twinsil, Picodent GmbH, Germany).

**Glass coatings for integrin-reconstituted GUVs adhesion experiments.** To validate the biological functionality of the reconstituted integrin after the process of release, the adhesion of the integrin-reconstituted GUVs to fibrinogen-, fibronectin-, collagen-, and BSA-coated glass surfaces was examined and compared (Supplementary Figure 8). Therefore, dsGUVs with reconstituted  $\alpha_{\text{IIb}}\beta_3$  integrin were formed and released as described in (Online Methods). For adhesion experiments integrin activation buffer (20 mM TRIS/HCl, pH 7.4, 50 mM NaCl, 0.5 mM  $\text{CaCl}_2$ , 1 mM  $\text{MnCl}_2$  and 1 mM  $\text{MgCl}_2$ ) was used inside and outside the GUVs. Following release the integrin-reconstituted GUVs were transferred to an observation chamber (Supplementary Figure 5) containing fibrinogen-, fibronectin-, collagen-, or BSA-coated glass slides. The adhesion was analyzed after 8 h incubation at  $4^\circ\text{C}$  to allow the integrin to interact with the different coatings. For these experiments fibronectin isolated from human plasma<sup>8</sup> was dissolved in PBS, collagen Type I (calf skin, Sigma-Aldrich, Germany) was dissolved in 0.1 M acetic acid and fibrinogen (human plasma, Merck Millipore, Germany) was first dissolved in 8.5% NaCl and for the incubation transferred to PBS.

For coating the glass surface of the observation chamber, pretreated glass slides ( $\text{O}_2$  plasma, 200 W, 30 s) were incubated with 0.1 mg/ml protein solution ( $8.5 \mu\text{g}/\text{cm}^2$ ) over night at  $4^\circ\text{C}$  (fibrinogen and collagen) or 1.5 h at room temperature (fibronectin). For the BSA coating the glasses were incubated with 10 mg/ml BSA in PBS for 2 h at room temperature, followed by a washing step with PBS and water for each 5 min. After incubation, the glass slides were air dried over night at  $4^\circ\text{C}$ . The coverslips for the observation chamber were passivated with BSA.

**Microscopy.** All experiments were performed on a Leica SP5 confocal microscope (Leica Microsystems, Germany) equipped with an argon and a white light laser. The measurements were conducted at  $25^\circ\text{C}$  and in case of microtubule analysis at  $37^\circ\text{C}$ . Droplets, sealed in an analysis chamber, were observed via a 63x oil objective (HCX PL APO 63x/1.40-0.60; Leica Microsystems GmbH, Germany). Fluorophores were excited at 488, 550 and 555 nm and the detection windows were set at 498-540 and 560-620 nm and 565-625 nm in case of ATTO 488, Rhodamine B and TAMRA-labeling, respectively. The pinhole for data acquisition was set to 1 Airy unit, which corresponds to an Airy disk diameter of  $96 \mu\text{m}$  and  $0.9 \mu\text{m}$  thickness of the optical slice.

**FRAP measurements.** Due to the density differences between the aqueous droplets and the surrounding oil ( $1.0 \times 10^3$  vs.  $1.9 \times 10^3 \text{ kgm}^{-3}$ ), the droplets ascend towards the upper slide of the observation chamber (Supplementary Figure 5). In this position, the droplets were scanned in z-direction until the bottom slice of the droplet was identified. The base of the droplet was chosen as a focal plane for FRAP measurements in order to exclude any influence from the cover slip at the chamber ceiling. A circular spot with a diameter of  $5 \mu\text{m}$  was selected as the bleaching area. It should be noted that in case of FRAP measurements performed inside the droplets or on their periphery the actual bleaching area was measured and corrected for each measurement due to distortion of the optical path as a reason of diffraction/refraction at the

oil/water interface. Time course of each FRAP experiment included 10 pre-bleaching images, 2 to 10 bleach cycles to eliminate the fluorescent signal and 50 to 200 post-bleaching images to record the fluorescence recovery. The bleaching time was adjusted to each fluorophore and laser used in the experiments, the acquisition frequency of post-bleaching images was adapted to the total recovery time. The average diffusion coefficient for each experiment and its standard error were calculated from at least 20 measurements. The analysis followed the protocols proposed by Axelrod et al.<sup>9</sup> and Soumpasis<sup>10</sup> as described in Supplementary Note 3.

**Raman spectroscopy.** For Raman spectra collection released GUVs or dsGUVs were injected into the observation chamber (Supplementary Figure 5). GUVs or dsGUVs, sealed in an analysis chamber, were observed via a 100x oil objective (NA 1.2, Zeiss, Germany) using a confocal Raman microscope (Alpha300RA, WITec GmbH, Germany). To collect Raman scattered light, the same objective was used for focusing a 532 nm laser (20 mW, spot size 350 nm) onto single GUVs or dsGUVs. The acquisition time was fixed to 2.14 seconds with five accumulations for each collection window. At the end of spectra collection the location of the observed subject was investigated and, in case the location was preserved the collected data was saved. The representative Raman spectra of the dsGUVs and of the released GUVs can be observed in Supplementary Figure 7.

**Fluctuation analysis.** Fluctuation analysis was performed following the protocol described earlier.<sup>11</sup> The GUVs were placed in a chamber made of two cover slips and a 2 mm-thick ring made of Teflon, and observed under phase contrast. The data was acquired at room temperature ~23°C. The acquisition of five thousands of snapshots was done by high-resolution camera (pco.edge, PCO AG, Kelheim, Germany). More than 10 vesicles per type of sample were examined.

The bending rigidity of vesicles released from droplets was measured and compared to that of vesicles prepared following the method of electroformation<sup>12, 13</sup> or gel-assisted swelling.<sup>14</sup> The membrane composition was DOPC:POPC:Chol (4:4:2) in mole ratios and small amount of the ATTO 488 labeled DOPE was also added at concentration of 1 mol% of total lipid. The buffer composition used for fluctuation analysis of the released GUVs was adjusted to be similar to integrin activation buffer within the GUVs (20 mM TRIS/HCl, pH 7.4, 50 mM NaCl, 0.5 mM CaCl<sub>2</sub>, 1 mM MnCl<sub>2</sub> and 1 mM MgCl<sub>2</sub>). The bending rigidity of the released vesicles was measured to be  $21.5 \pm 3.4$  k<sub>B</sub>T (standard deviation). This value lies in the range of typical values reported for the bending rigidity of PC membranes,<sup>15</sup> suggesting that the bilayers are clean of impurities. The methods of electroformation and gel-assisted swelling did not yield suitable vesicles (the vesicles were small and with defects or multilamellar) when grown in the buffer used for the preparation of dsGUVs. Therefore, we electroformed vesicles with the same membrane composition but in solution of 1 mM MgCl<sub>2</sub>. The bending rigidity values for these membranes were found to be  $25.3 \pm 3.0$  k<sub>B</sub>T ideally corresponding to the data for released vesicles.

## Supplementary Notes

### Supplementary Note1. Calculation of minimal lipid concentration required to form a continuous lipid bilayer inside droplets - dsGUV:

The following lipid concentration calculation is done for droplets with 75 μm radius. The volume  $V_{droplet}$  and the surface area  $A_{droplet}$  of a spherical droplet is given by

$$V_{\text{droplet}} = \frac{4}{3}\pi r^3 = 1.8 \times 10^6 \mu\text{m}^3 = 1.8 \text{ nL}$$

and

$$A_{\text{droplet}} = 4\pi r^2 = 7.1 \times 10^{10} \text{ nm}^2.$$

Assumption: Average area occupied by a single phospholipid in a lipid membrane equals<sup>16</sup>

$$A_{\text{headgroup}} = 0.7 \text{ nm}^2.$$

The amount of lipids per droplet needed to form a complete lipid bilayer is therefore:

$$N_{\text{lipids}} = 2 * A_{\text{droplet}} / A_{\text{headgroup}} = 2.3 \times 10^{11}.$$

Thus, the lipid concentration required to form a lipid bilayer inside droplets is

$$c = \frac{N_{\text{lipids}}}{V_{\text{droplet}} * N_A} = \frac{6}{r * N_A * A_{\text{headgroup}}} = 190 \mu\text{M}.$$

The concentration for droplets with different radii used in this study is  $c(r=50 \mu\text{m}) = 285 \mu\text{M}$  and  $c(r=20 \mu\text{m}) = 712 \mu\text{M}$ .

For the experiments an excess of  $\approx 15\%$  in lipid concentration was used for the following two reasons: 1) to compensate for possible lipids loss during the production; and 2) to compensate for volume increase due to pico-injection.

To validate experimentally the relevance of theoretically estimated lipid concentration, we systematically varied the amount of fluorescently-labeled lipids injected into monodisperse droplets and recorded their fluorescence intensity at the droplet interface. In case of minor lipid amount which would not cover the complete inner surface of the droplet we did not see the assembly of smaller GUVs than the size of the droplet itself. Instead we observed fusion of available lipids at the inner wall of the droplet. A plot of the measured data is shown in Supplementary Figure 1. Considering the diameter of  $120 \mu\text{m}$  of the droplets used in this experiment, a calculated concentration of  $237 \mu\text{M}$  lipids is required for full bilayer coverage. As can be observed in Supplementary Figure 1, the intensity values are increasing approximately linear up to the theoretical estimated concentration. At elevated concentration the intensity reaches a plateau. It should be noted that at higher concentrations the excess lipids form aggregates of liposomes at the droplet interface. Inhomogeneous aggregation of liposomes on the droplet's periphery affecting precise estimation of the intensity. Therefore, higher deviation in the recorded intensity at  $500 \mu\text{M}$  is attributed to this effect.

### Supplementary Note 2. Calculation of vesicle diffusion in microfluidic droplets

Assuming 3D Brownian motion, the mean square displacement  $\langle r^2(t) \rangle$  of a particle in solution is

$$\langle r^2(t) \rangle = 6D\langle t \rangle.$$

The mean time  $\langle t \rangle$  needed for the particle to travel the distance  $\sqrt{\langle r^2(t) \rangle}$  is therefore

$$\langle t \rangle = \frac{\langle r^2(t) \rangle}{6D}$$

The diffusion coefficient  $D$  of a spherical particle with radius  $R$  in a solution with viscosity  $\eta$  for a given temperature  $T$  is

$$D = \frac{k_B T}{6\pi\eta R}$$

Therefore, the average time for a vesicle with radius  $R$  needed to diffuse from the center of the droplet to the periphery ( $\sqrt{\langle r^2(t) \rangle} = 20 \mu\text{m}$ ) is

$$\langle t \rangle = \frac{\langle r^2(t) \rangle}{6} \frac{6\pi\eta R}{k_B T}$$

Assuming an aqueous solution with  $\eta = 0.1 \text{ Pa} \cdot \text{s}$  and a temperature  $T = 25^\circ\text{C}$ , the average time for all vesicle to diffuse from the centrum to the periphery of the droplet with diameter  $40 \mu\text{m}$  is

$$\langle t(R = 50 \text{ nm}) \rangle \approx 15 \text{ s}$$

and

$$\langle t(R = 5 \mu\text{m}) \rangle \approx 25 \text{ min.}$$

### Supplementary Note 3. Evaluation of FRAP data

The analysis followed a protocol proposed by Axelrod et al.<sup>9</sup> and Soumpasis.<sup>10</sup> To correct the background noise  $I_{bg}$ , the detector signal was measured in the oil phase using the same settings as for the FRAP measurements.  $I_{bg}$  was subsequently subtracted from all the measured intensity values. Average intensity values of the bleaching spot,  $I(t)$ , and as a reference of the whole droplet base,  $T(t)$ , were extracted from the recorded images.  $I(t)$  and  $T(t)$  were normalized by the averages of the prebleaching values,  $I_{pb}$  and  $T_{pb}$ . To correct for photofading the intensities of the bleached spot were multiplied with the reciprocal, normalized intensities of the droplet base,  $T(t)$ . Thus the normalized and corrected intensities,  $I_{nor}$ , were calculated as

$$I_{nor} = \frac{I(t) - I_{bg}}{I_{pb} - I_{bg}} \frac{T_{pb} - I_{bg}}{T(t) - I_{bg}}$$

A nonlinear least-square fit was then applied using MATLAB R2015a SP1 (Mathworks, USA) to fit an exponential function  $f(t)$ ,

$$f(t) = a(1 - \exp(\lambda \cdot t)),$$

to the normalized intensities,  $I_{nor}$ . The resulting values of the coefficient  $\lambda$  were then used to calculate the half-recovery time  $\tau_{1/2}$  for each bleaching experiment,

$$\tau_{1/2} = \frac{-\log(0.5)}{\lambda}$$

The diffusion coefficient,  $D$ , is related to the half-recovery time  $\tau_{1/2}$  via the square radius of the bleaching spot, assuming Gaussian bleaching profile,

$$D = 0.32 \frac{r^2}{\tau_{1/2}}$$

The average diffusion coefficient for each experiment and its standard error were calculated from at least 20 measurements (Supplementary Figure 9).

#### Supplementary Note 4. Calculation of number of integrin proteins that might be reconstituted in dsGUVs.

Droplet surface area:

$$S(r = 20\mu\text{m}) = 5026 \mu\text{m}^2$$

$$S(r = 50\mu\text{m}) = 31416 \mu\text{m}^2$$

Area of a lipid in a membrane (from literature)

$$A_{lip} \approx 0.7\text{nm}^2$$

Cross-section of the transmembrane domain of integrin (two  $\alpha$  helices).<sup>17</sup>

$$A_{int} = 2\text{nm}^2$$

Integrin/Lipid Ratio	Surface area of lipid bilayer with one reconstituted integrin.	$N_{int}$ ( $r = 20\mu\text{m}$ )	$N_{int}$ ( $r = 50\mu\text{m}$ )
1:1000	$\frac{1000 * 0.7\text{nm}^2}{2} + 2\text{nm} = 352\text{nm}^2$	$1.43 * 10^7$	$8.92 * 10^7$
1:10,000	$\frac{10,000 * 0.7\text{nm}^2}{2} + 2\text{nm} = 3502\text{nm}^2$	$1.44 * 10^6$	$8.97 * 10^6$

#### Supplementary Note 5. Matlab code for FRAP analysis

```

*****
% FRAP evaluation
% version 5 20161010
% Matlab-script for the evaluation of FRAP data. This script is designed to to evaluate '.csv' files
exported
% using the Leica Microscopy Software. For correct evaluation the files should contain
% three columns, first the intensity values form the bleaching spot, second a reference spot
% and a thrid a larger area containing the bleaching spot. The data sets can differ in time steps
and total
% number of datapoints. The script will output the computed diffusion coefficient for each dataset
as well
% the average diffusion coefficient and it's corresponding standard error. Optionally the script
will draw
% graphs of each evaluation step.

%Program timer
%tic

*****
% A set of parameters that control the evaluation of the results
% Plotting switch. If value is true all intermediary results are plotted into
% pdf files. This slows down script drastically
plotall = true ;
% Radius of the bleached spot in Åµm. Important for the evaluation of the
% diffusion coefficient
w = 2.5;
% For good results its important, to correct the collected data points for background.
bg=0;
% The calculation is on standard done according to protocols published by Axelrod et al. (1976) and
Soumpasis (1983).
% Alternatively a model proposed by Kang et al. (2012) can be used, correcting for diffusion during
the bleaching.
% To derive the prefactor the script 'Frap radius evaluation.m' can be used.
pf=0.32;

*****
% Main body of code
*****

```

```

%% Importing the data and removing rows with empty cells
files = dir('*.*.csv');
for i=1:length(files)
    data=importdata(files(i).name);
    J=all(~isnan(data.data),2);
    A{i}=data.data(J,:);
    clear data J
end

%%%%%%%%%%%%%%%%%%%%%%%%%%%%%%%%%%%%%%%%%%%%%%%%%%%%%%%%%%%%%%%%%%%%%%%%
%% Plotting of raw data
if plotall == true
for i=1:length(files)
    figure('vis', 'off');
    plot1=plot(A{i}(:,1),A{i}(:,2:4), 'LineStyle','none');
    set(plot1(1), 'Marker', 'o', 'DisplayName', 'ROI1');
    set(plot1(2), 'Marker', '.', 'DisplayName', 'ROI2');
    set(plot1(3), 'Marker', 'x', 'DisplayName', 'ROI3');
    xlabel('time [s]');
    ylabel('intensity');
    title(files(i).name)
    print(sprintf('raw%02d',i) , '-dpdf')
end
end

%%%%%%%%%%%%%%%%%%%%%%%%%%%%%%%%%%%%%%%%%%%%%%%%%%%%%%%%%%%%%%%%%%%%%%%%
%% Data correction and normalization
% Each dataset is corrected for background, normalized by the prebleaching value
% and corrected for photofading in this step
for i=1:length(files)
    B{i}=zeros(length(A{i}),2);
    %% Mean intensity of focus point before bleach
    Ipre=mean(A{i}(1:10,2));
    %% Mean intensity of the total cell before bleach
    Tpre=mean(A{i}(1:10,4));
    %% Calculating normalized values (without background substration)
    B{i}(:,1)=A{i}(:,1);
    B{i}(:,2)=(A{i}(:,2)-bg)./(Ipre-bg) * (Tpre-bg) ./ (A{i}(:,4)-bg);
end

clear i j A Ipre Tpre bg

%%%%%%%%%%%%%%%%%%%%%%%%%%%%%%%%%%%%%%%%%%%%%%%%%%%%%%%%%%%%%%%%%%%%%%%%
%% Plotting normalized graphs
if plotall == true
for i=1:length(files)
    figure('vis', 'off');
    plot(B{i}(:,1),B{i}(:,2), 'Marker', 'o', 'LineStyle', 'none', 'DisplayName', 'B(:,1.6)');
    xlabel('time [s]');
    ylabel('intensity');
    title(files(i).name)
    print(sprintf('normalized%02d',i) , '-dpdf')
end
clear i
end

%%%%%%%%%%%%%%%%%%%%%%%%%%%%%%%%%%%%%%%%%%%%%%%%%%%%%%%%%%%%%%%%%%%%%%%%
%% Initialization of the fitting model
% As fitting function an exponential recovery curve is chosen. A robust, non-linear least square has
proven to
% show good results. The fit outputs information about the fit quality to allow debugging.
fo = fitoptions('method','NonlinearLeastSquares','Lower',[0 0], 'Upper',[1 Inf],
'Robust','Bisquare');
st = [1 1]; %starting point
set(fo, 'Startpoint', st);
ft = fittype('a*(1-exp(-t*b))', ...
'dependent', {'y'}, 'independent', {'t'}, ...
'coefficients', {'a', 'b'});

%%%%%%%%%%%%%%%%%%%%%%%%%%%%%%%%%%%%%%%%%%%%%%%%%%%%%%%%%%%%%%%%%%%%%%%%
%% The normalized data is fitted to the previously initialized fitting model. The results are
directly plotted.
C=zeros(2,length(files));
for i=1:length(files)
    [cf,gof] = fit(B{i}(11:length(B{i}),1)-B{i}(11,1),B{i}(11:length(B{i}),2)-B{i}(11,2),ft,fo);
    C(:,i) = transpose(coefvalues(cf));
    if plotall == true
        figure('vis', 'off')
        hold on
        ylim([-0.05 0.2])
        plot(B{i}(:,1)-B{i}(11,1),B{i}(:,2)-
B{i}(11,2), 'Marker', 'o', 'LineStyle', 'none', 'DisplayName', 'B(:,1.6)');
        plot(cf);
        xlabel('time [sec]', 'FontSize', 20)
        ylabel('normalized fluorescence Intensity', 'FontSize', 20)
        title(files(i).name)
        print(sprintf('fitted%02d',i) , '-dpdf')
    end
    clear cf gof
end

clear i st fo ft plotall B

%%%%%%%%%%%%%%%%%%%%%%%%%%%%%%%%%%%%%%%%%%%%%%%%%%%%%%%%%%%%%%%%%%%%%%%%

```

```

%% Calculation of diffusion coefficients
% The values are computed from the fitting results and the size of the bleaching spot. They are
% first calculated for each dataset separately and then the average and standard error is computed.
% The calculation is on standard done according to protocols published by Axelrod et al. (1976) and
Soumpasis (1983).
% Alternatively a model proposed by Kang et al. (2012) can be used, correcting for diffusion during
the bleaching
tauh=-log(0.5)./C(2,:);
C(3,:)=pf*w^2./tauh;
D=[mean(C(3,:)),std(C(3,:))/sqrt(length(C(3,:)))];

%%%%%%%%%%%%%%%%%%%%%%%%%%%%%%%%%%%%%%%%%%%%%%%%%%%%%%%%%%%%%%%%%%%%%%%%
%% Saving the results
save coefficients.txt C -ASCII
fid=fopen('diffusion_coefficient.txt','w');
fprintf(fid,'diffusion_coefficient std_error [Åm^2/s]\n');
fprintf(fid,'%f %f',D);
close

clear files w fid tauh pf

%toc

```

## Supplementary Note 6. Matlab code for fluorescence intensity analysis

```

%%%%%%%%%%%%%%%%%%%%%%%%%%%%%%%%%%%%%%%%%%%%%%%%%%%%%%%%%%%%%%%%%%%%%%%%
%% Droplet intensity profile evaluation script
% version 4 20161205
% As there is refraction and defraction on the water oil interface of the droplets,
% it is difficult to compare the fluorescence intensity of GUV and dsGUV. This script
% tries to solve this problem by fitting and integrating the fluorescence
% intensity profile. This script is designed to to evaluate '.csv' files exported
% using the Leica Microscopy Software

%%%%%%%%%%%%%%%%%%%%%%%%%%%%%%%%%%%%%%%%%%%%%%%%%%%%%%%%%%%%%%%%%%%%%%%%
%% A set of parameters that control the evaluation of the results
% Plotting switch. If value is true all intermediary results are plotted into
% pdf files. This slows down script drastically
plotall = true;

%%%%%%%%%%%%%%%%%%%%%%%%%%%%%%%%%%%%%%%%%%%%%%%%%%%%%%%%%%%%%%%%%%%%%%%%
%% Main body of code
%%%%%%%%%%%%%%%%%%%%%%%%%%%%%%%%%%%%%%%%%%%%%%%%%%%%%%%%%%%%%%%%%%%%%%%%

%%%%%%%%%%%%%%%%%%%%%%%%%%%%%%%%%%%%%%%%%%%%%%%%%%%%%%%%%%%%%%%%%%%%%%%%
%% Importing the data and removing rows with empty cells
files = dir('*.csv');
for i=1:length(files)
    data=importdata(files(i).name);
    J=all(~isnan(data.data),2);
    A{i}=data.data(J,:);
    clear data J
end

%%%%%%%%%%%%%%%%%%%%%%%%%%%%%%%%%%%%%%%%%%%%%%%%%%%%%%%%%%%%%%%%%%%%%%%%
%% Plotting of raw data
if plotall == true
    for i=1:length(files)
        figure('vis','off');
        hold on
        plot1=plot(A{i}(:,3),A{i}(:,4));
        set(plot1(1),'Marker','o','DisplayName','ROI1');
        xlabel('position [Åm]');
        ylabel('intensity');
        title(files(i).name,'FontSize',24)
        print(sprintf('raw%02d',i),'-dpdf')
    end
end

%%%%%%%%%%%%%%%%%%%%%%%%%%%%%%%%%%%%%%%%%%%%%%%%%%%%%%%%%%%%%%%%%%%%%%%%
%% Fitting of Gaussian functions to the peaks
% The data is split in two arrays around each peak and fitted with Gaussian functions
B=zeros(length(files)*2,2);

%%%%%%%%%%%%%%%%%%%%%%%%%%%%%%%%%%%%%%%%%%%%%%%%%%%%%%%%%%%%%%%%%%%%%%%%
%% Finding good starting points
% Searches for the position and values of two intensity peaks of a droplet crossection.
for i=1:length(files)
    j=round(length(A{i})/2);
    [m1 p1]=max(A{i}(1:j,4));
    [m2 p2]=max(A{i}(j:length(A{i}),4));
    B(i*2-1,1)=m1;
    B(i*2,1)=m2;
%%%%%%%%%%%%%%%%%%%%%%%%%%%%%%%%%%%%%%%%%%%%%%%%%%%%%%%%%%%%%%%%%%%%%%%%
%% Fitting a Gaussian function to the data via a nonlinear least square to the 'left' peak
% The fit uses the previously derived values as starting points
fo = fitoptions('method','NonlinearLeastSquares','Lower',[0 0 0 2],'Upper',[100 A{i}(j,3) 1e-4
3], 'Robust','Bisquare');
st = [m1 A{i}(p1,3) 1e-6 2.2]; %starting point
set(fo,'Startpoint',st);

```

```

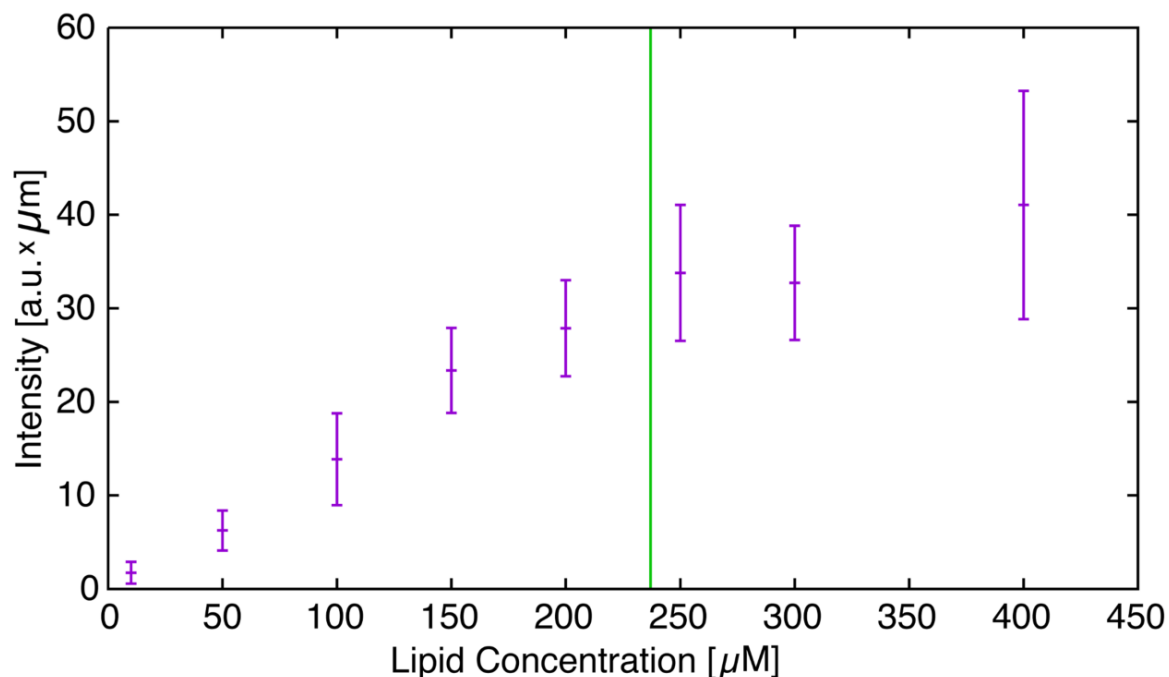
ft = fitype('a1*exp(-(x-b1)/c1)^2 +c3',...
            'dependent',{'y'},'independent',{'x'},'coefficients',{'a1','b1','c1','c3'});
x=A{i}(1:j,3);
y=A{i}(1:j,4);
f1=fit(x,y,ft,fo);
c=coeffvalues(f1);
B(i*2-1,2)=c(1)*c(3)*pi^.5;
clear c
%%%%%%%%%%%%%%%%%%%%%%%%%%%%%%%%%%%%%%%%%%%%%%%%%%%%%%%%%%%%%%%%%%%%%%%%
%% Fitting a Gaussian function to the data via a nonlinear least square to the 'right' peak
% The fit uses the previously derived values as starting points
fo = fitoptions('method','NonlinearLeastSquares','Lower',[0 A{i}(j,3) 1e-10 2],'Upper',[100
A{i}(length(A{i}),3) 1e-4 3], 'Robust','Bisquare');
st = [m2 A{i}(p2+j,3) 1e-6 2.2];
set(fo,'Startpoint',st);
x=A{i}(j:length(A{i}),3);
y=A{i}(j:length(A{i}),4);
f2=fit(x,y,ft,fo);
c=coeffvalues(f2);
B(i*2,2)=c(1)*c(3)*pi^.5;
clear c
%%%%%%%%%%%%%%%%%%%%%%%%%%%%%%%%%%%%%%%%%%%%%%%%%%%%%%%%%%%%%%%%%%%%%%%%
%% Plotting of data with fitting results
if plotall == true
    figure('vis','off');
    hold on
    plot(A{i}(:,3),A{i}(:,4));
    plot(f1);
    plot(f2);
    xlabel('position [um]','FontSize',20)
    ylabel('Intensity','FontSize',20)
    title(files(i).name,'FontSize',24)
    print(sprintf('fitted%02d',i), '-dpdf')
end
clear x y j m1 m2 p1 p2 fo ft f1 f2 i st c
end
%%%%%%%%%%%%%%%%%%%%%%%%%%%%%%%%%%%%%%%%%%%%%%%%%%%%%%%%%%%%%%%%%%%%%%%%
%% Calculation of maximal intensity values and integrated intensity
% The columns contain in order: the mean maximal values, the corresponding standard error,
% the integrated intensity, and the corresponding standard error.
C(1,1)=mean(B(:,1));
C(1,2)=std(B(:,1))/sqrt(length(files));
C(1,3)=mean(B(:,2))*10^6;
C(1,4)=std(B(:,2))*10^6/sqrt(length(files));

%%%%%%%%%%%%%%%%%%%%%%%%%%%%%%%%%%%%%%%%%%%%%%%%%%%%%%%%%%%%%%%%%%%%%%%%
%% Saving the results
fid = fopen('intensity_values.txt', 'w');
fprintf(fid, 'max intensity [au] std error [au] integrated intensity [au*um] std error
[au*um]\n %f %f %f %f',C);
close

clear plotall files ans plot1 fid

```

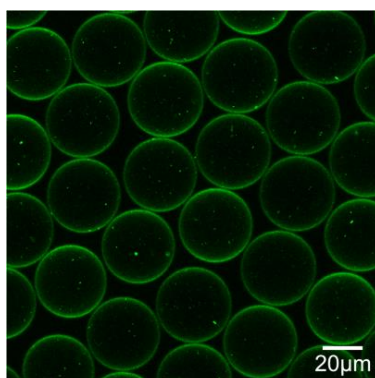
## Supplementary Figures



## Supplementary Figure 1

Fluorescence intensity of the lipids at the droplets interface as a function of encapsulated lipid concentration.

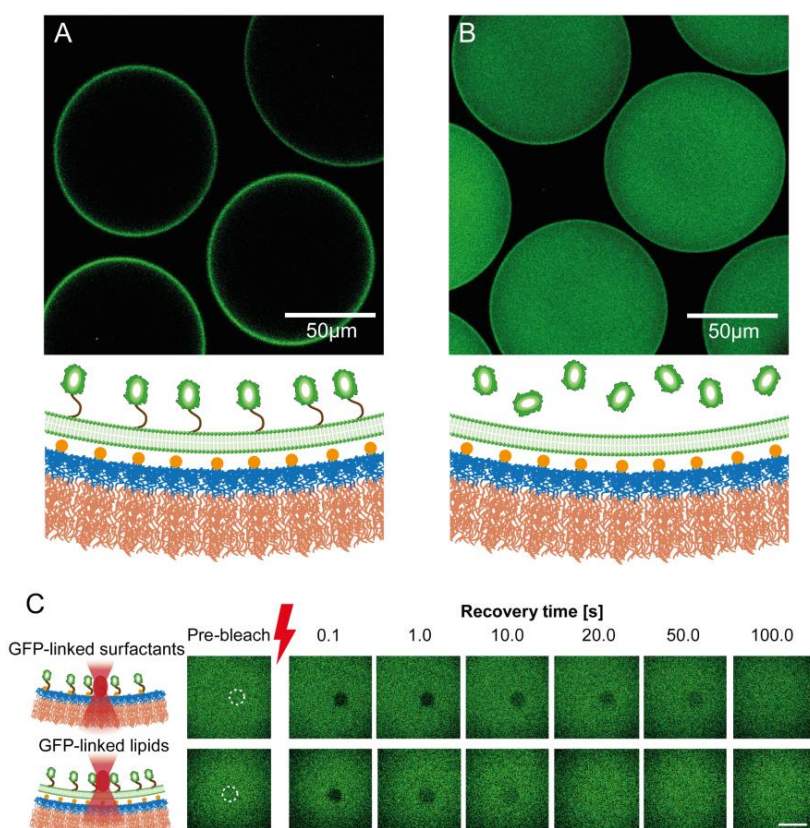
To validate experimentally the relevance of theoretically estimated lipid concentration (237  $\mu\text{M}$ , Supplementary Note 1), we systematically varied the amount of fluorescently-labeled lipids (egg PC:egg PG, 9:1, including 0.5 % ATTO 488-labelled DOPE) encapsulated into 120  $\mu\text{m}$  diameter monodisperse droplets and recorded their fluorescence intensity at the droplet interface. In case of lipid concentration lower than 237  $\mu\text{M}$  no smaller GUVs than the size of the droplet itself were observed. Instead fusion of available lipids at the inner wall of the droplet was detected. As can be observed, the lipid fluorescence intensity values are increasing approximately linear up to the theoretical estimated concentration. At higher lipid concentration the intensity reaches a plateau. It should be noted that at higher concentrations the excess lipids form aggregates of liposomes at the droplet interface. Inhomogeneous aggregation of liposomes on the droplet's periphery affecting precise estimation of the intensity. Therefore, higher deviation in the recorded intensity at 400  $\mu\text{M}$  lipid concentration is attributed to this effect. The mean integrated intensity values and their standard deviation, indicated by the error bars, were derived from intensity profiles taken from twenty individual droplets, each intersecting the membrane twice rectangularly.



### Supplementary Figure 2

Partial vesicle fusion due to 10 mM  $\text{Ca}^{2+}$  ions addition.

Representative fluorescence image of lipid distribution (DOPC:DOPE:DOPS 8:1:1, including 1% ATTO 488-labeled DOPE) within microfluidic water-in-oil droplets, containing 10 mM  $\text{Ca}^{2+}$  ions ( $\text{CaCl}_2$ ), measured 1 h after creation.

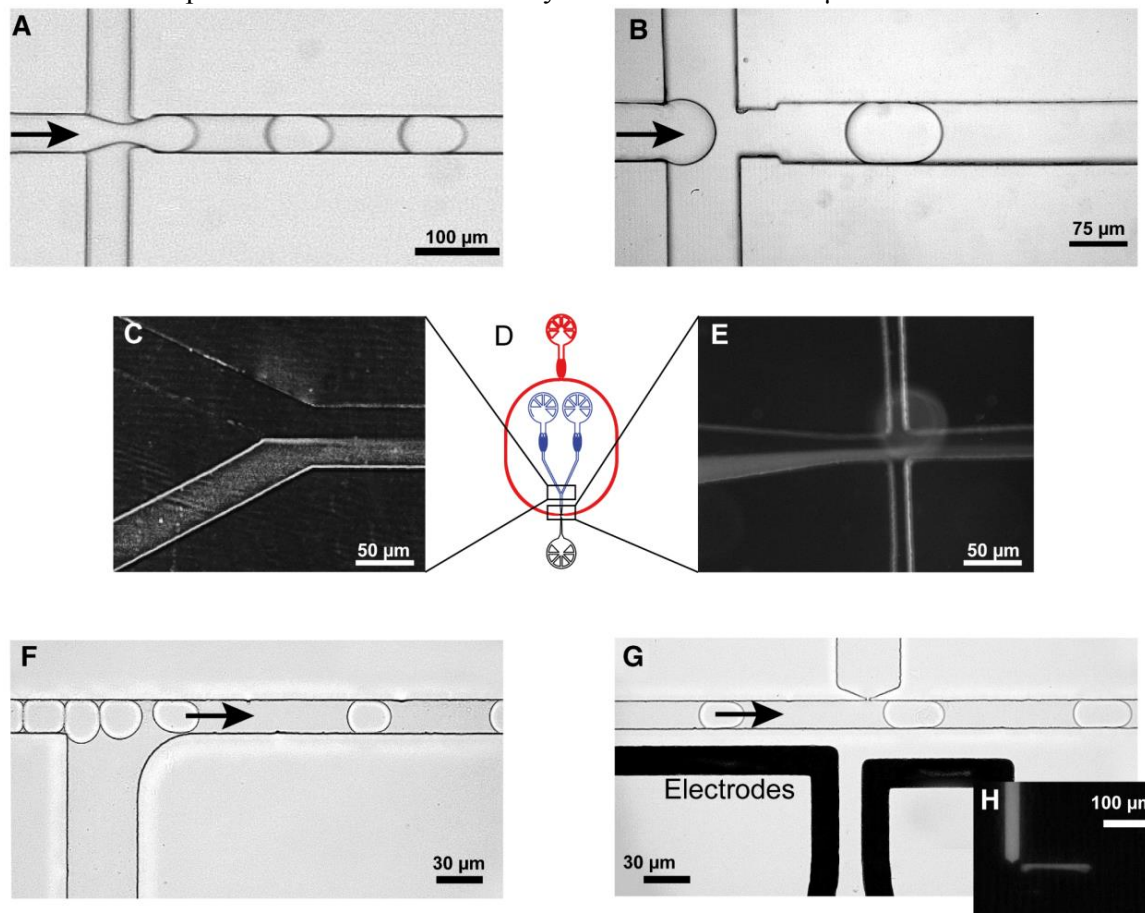


### Supplementary Figure 3

Biofunctionalization of dsGUVs via DGS-NTA(Ni)lipids.

In order to test the functionalization of dsGUVs, (His6)-GFP was pico-injected into droplets. (A) For droplets containing DOPC:DGS-NTA(Ni), 9:1 (220  $\mu\text{M}$ ), (His6)-GFP was linked to the dsGUVs at the droplets periphery. (B) An equally distributed fluorescence signal was observed when no anchoring points were present (here: dsGUVs consisting of DOPC lipids only). (C) Representative FRAP experiments on the mobility of (His6)-GFP immobilized to the

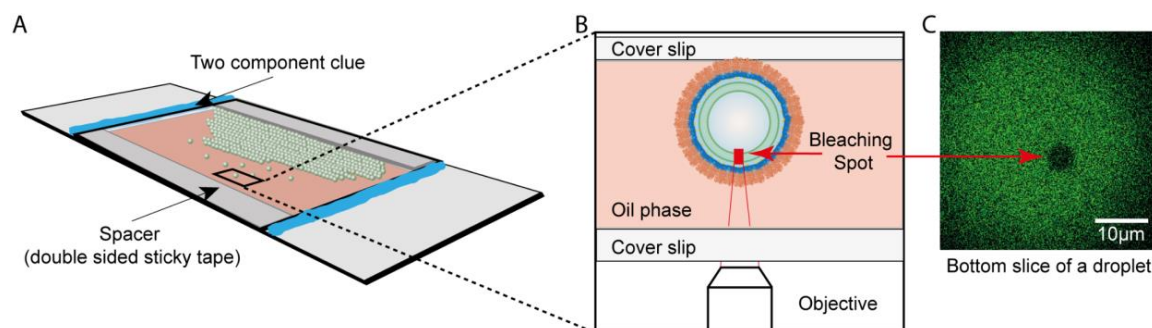
copolymer-stabilized droplet interface (upper trace) or the dsGUV (lower trace). The bleached area is encircled in the pre-bleach frame and the recovery time (seconds after bleaching) is indicated on top of the fluorescence recovery frames. Scale bar 10  $\mu\text{m}$ .



#### Supplementary Figure 4

Droplet-based microfluidic functional units.

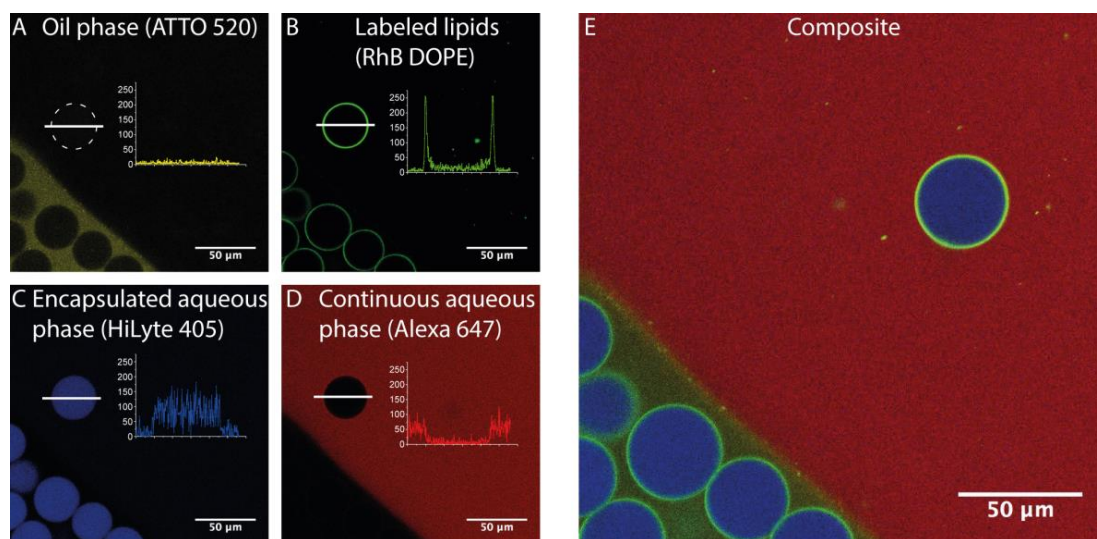
Presentation of different droplet-based microfluidic operating units used in this research. (A) and (B) show representative images of the flow-focusing junctions for droplets production with a diameter of 40 and 100  $\mu\text{m}$ , respectively. (D) shows a microfluidic droplet production device with two aqueous inlet channels (blue) and one oil channel (red). This device was implemented in actin-related experiments in order to avoid actin polymerization prior to droplet formation. Inset (C) and (E) show representative fluorescence images of the two phases for actin polymerization within the droplets. Bright phases represent the actin solution containing Alexa 488-labeled G-actin. The second phase contains all necessary bio-molecules for polymerization and bundling of actin. The solutions have a contact time in the millisecond range before getting encapsulated. Images (F) and (G) represent the pico-injection device for controlled introduction of different cellular components into droplets. (F) The spacing between the droplets carrying different biologically-active molecules is controlled through addition of oil via the second oil channel. (G) An alternating electric potential (1 kHz and 250 V) reduces the stability (poration) of the surfactants-lipid layer at the droplet interface for an aqueous injection of reagents from a pico-injection channel (injection volume can be ranged between 2 to 100 pl, dependent on the applied pressure). The injection process can be visualized by injection of ATTO 488-labeled  $F_0F_1$ -ATP synthase (H), using fluorescence microscopy.



### Supplementary Figure 5

Observation chamber and analysis setup.

(A) Shows the design of an observation chamber for droplet analysis. (B) Magnified cross-section representation of the analysis chamber. Due to the density differences, droplets rise to the top of the chamber. Confocal microscopy was used to scan the droplet in order to find the bottom plane. The lowest slice of the droplet was chosen as a focal plane for FRAP measurements in order to exclude any influence of stiff objects like in the case of the coverslip and the upper parts of the droplet. (C) Example of a FRAP experiment performed on dsGUV containing GFP-linked DGS lipids. The image shows a circular bleached spot with a 5  $\mu\text{m}$  diameter.

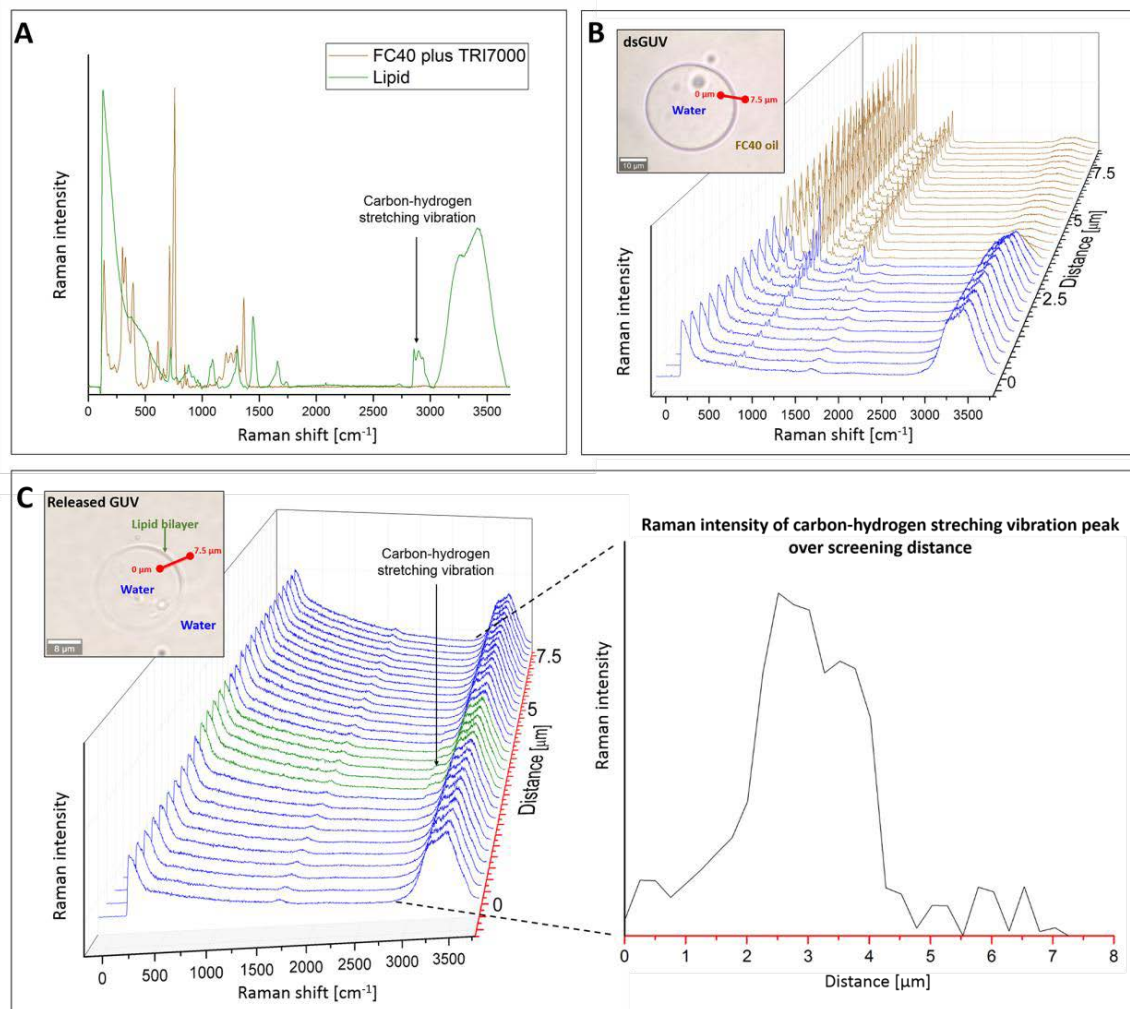


### Supplementary Figure 6

Release of dsGUVs, preservation of content and checking for oil residues.

To evaluate if the lipid bilayer stayed intact during the release process the (A) oil phase (ATTO 520, yellow), the (B) lipid bilayer (RhB DOPE, green), the (C) encapsulated (HyLite 405, blue) and (D) continuous water phase (Alexa 647, red) were labeled with distinctive fluorophores. (E) A composite image of all channels. On the bottom left of each frame is the continuous oil phase containing multiple dsGUV encapsulating aqueous medium. The remainder of the frame is filled with a continuous aqueous phase containing a single released GUV. (A-D) The insets display a line profile intersecting the released GUV along the indicated white line for the respective fluorophore. (A) In the oil channel, no traces of remaining oil can be detected on the released GUV. (B) The fluorescent signal of the RhB DOPE is stronger compared to the dsGUV.

This is likely due to reduced diffraction and refraction. (C) and (D) show that no mixing between the aqueous phases was detected.

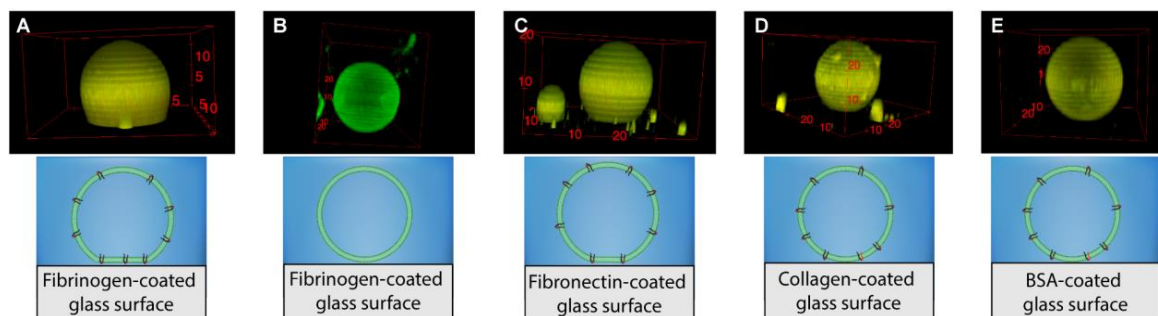


### Supplementary Figure 7

Raman spectra of dsGUVs and the released GUVs.

Raman microscope was used to perform Raman spectroscopy on released GUVs to provide a method for the detection of oil/surfactant residues in the released GUVs. (A) Comparison of Raman spectra collected from the solution of surfactants in FC40 oil (brown) and from the SUVs (green), consisting of 4:4:2 of DOPC, POPC and cholesterol, respectively. Carbon-hydrogen stretching vibration of lipid tails indicated by arrow between  $2800$  and  $3000\text{ cm}^{-1}$ .<sup>18</sup> The obtained FC40 oil spectrum in this study present similar peaks as published before.<sup>19</sup> (B) Representative Raman spectra collected through the water oil interphase of the single dsGUV as indicated by the red line in the insert bright-field image. In sake of clarity of presentation the spectra collected from the oil and water phases were brown and blue colored, respectively. (C) Representative Raman spectra collected through the water-lipid interphase of the released GUV as indicated by the red line in the insert bright-field image. In sake of clarity of presentation the spectra collected from the water phases and the lipid bilayer were blue and green colored, respectively. Importantly, no characteristic peaks of the FC40 oil/surfactant were detected

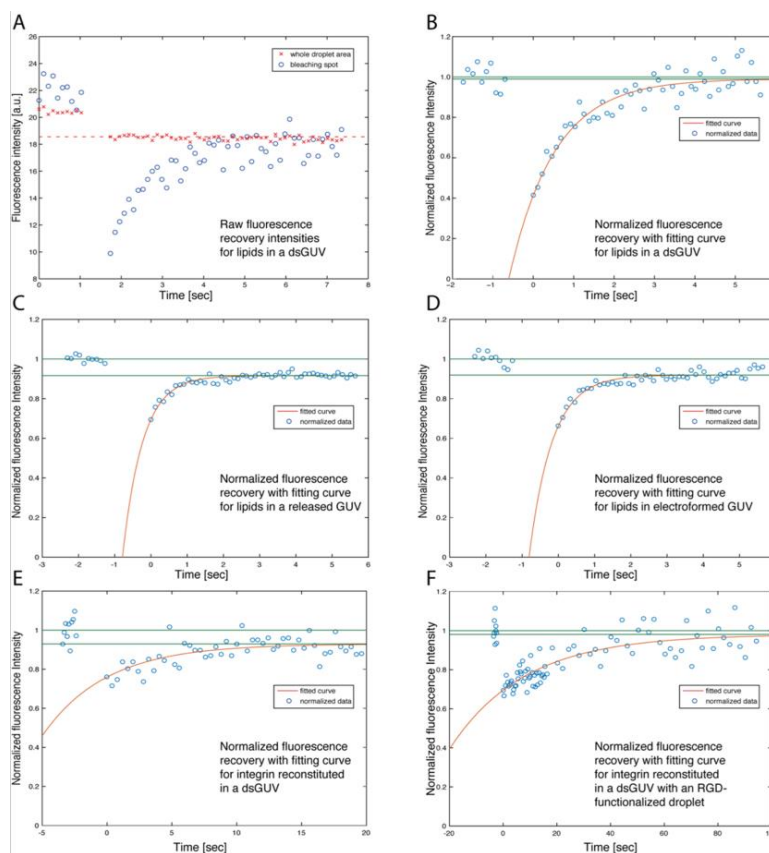
within the collected spectra. Raman intensity of the carbon-hydrogen stretching vibration of lipid tails (indicated by arrow) was plotted over the screening distance.



### Supplementary Figure 8

Release of integrin-reconstituted GUVs and their functionality assessment.

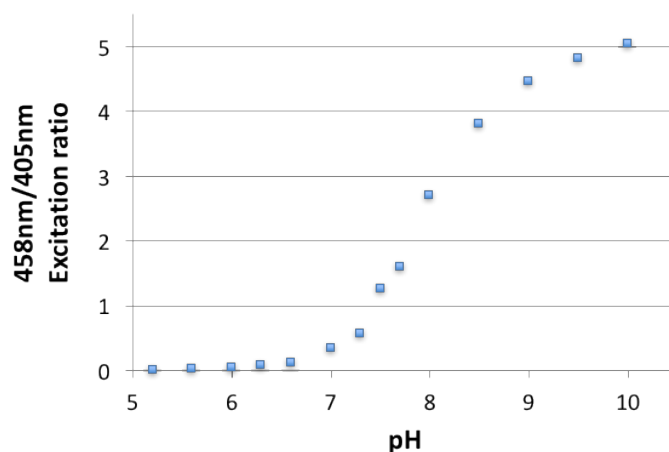
Representative 3D reconstruction of confocal images of recovered integrin-reconstituted GUVs and their interactions with (A) fibrinogen- (C) fibronectin- (D) collagen- and (E) BSA-coated glass surfaces. The integrin-reconstituted GUVs show strong or moderate adhesion to fibrinogen- or fibronectin-coated glass surfaces, respectively. In comparison, only very weak to no interaction was detected for collagen or BSA-coated surfaces. The merged fluorescence signals consist of ATTO 488-labeled DOPE lipids and TAMRA-labeled  $\alpha_{11b}\beta_3$  integrin. (B) Shows the control experiment in which due to the absence of reconstituted integrin no interaction between the GUV and the fibrinogen-coated glass surface was observed.



### Supplementary Figure 9

Representative recovery curves.

(A) Shows representative raw data acquired for a FRAP measurement on a dsGUV. The data consists of the average intensity values of the bleaching spot and of the whole droplet area in focus. A horizontal dotted line was added as a guide for the eye to indicate photo-fading. Before analysis, all data points were corrected for background. Furthermore, data points were normalized by the average pre-bleaching value and the inverse of the average intensity of the whole droplet in focus was multiplied to the values of the bleaching spot, to correct for photo-fading. The resulting normalized intensity values of the fitting points and fitting curve are presented for the same dsGUV (B). Representative normalized fluorescence recovery curves obtained from the measurements performed on released and produced by electroformation GUVs are presented (C) and (D), respectively. In the FRAP measurements as presented in A-D the same lipid composition containing 0.5 % ATTO 488-labeled DOPE was used as fluorescent marker. (E) and (F) show represented normalized fluorescence recovery curves obtained from the measurements performed on reconstituted TAMRA-labeled integrin proteins in dsGUVs with and without interaction with RGD peptides on the surfactant layer, respectively.



### Supplementary Figure 10

Pyranine as a pH sensor within the dsGUVs.

Pyranine was used as a sensor to monitor changes of the dsGUV internal pH. To calibrate the system, dsGUVs were produced with a given pH ranging from 5 to 10 with 1  $\mu$ M pyranine in the aqueous solution. These dsGUVs were then excited at 405 nm and 458 nm wavelength. The figure shows the variation of the fluorescence intensity ratios as a function of a given pH.

### Supplementary References

1. Johnson, J.M., Ha, T., Chu, S. & Boxer, S.G. Early Steps of Supported Bilayer Formation Probed by Single Vesicle Fluorescence Assays. *Biophys. J.* **83**, 3371-3379 (2002).
2. Herold, C., Chwastek, G., Schwille, P. & Petrov, E.P. Efficient Electroformation of Supergiant Unilamellar Vesicles Containing Cationic Lipids on ITO-Coated Electrodes. *Langmuir* **28**, 5518-5521 (2012).

3. Platzman, I., Janiesch, J.-W. & Spatz, J.P. Synthesis of Nanostructured and Biofunctionalized Water-in-Oil Droplets as Tools for Homing T Cells. *J. Am. Chem. Soc.* **135**, 3339-3342 (2013).
4. Janiesch, J.W. et al. Key factors for stable retention of fluorophores and labeled biomolecules in droplet-based microfluidics. *Anal Chem* **87**, 2063-2067 (2015).
5. Gu, H., Duits, M.H.G. & Mugele, F. Droplets Formation and Merging in Two-Phase Flow Microfluidics. *International Journal of Molecular Sciences* **12**, 2572-2597 (2011).
6. Xia, Y. & Whitesides, G.M. SOFT LITHOGRAPHY. *Annual Review of Materials Science* **28**, 153-184 (1998).
7. Abate, A.R., Hung, T., Mary, P., Agresti, J.J. & Weitz, D.A. High-throughput injection with microfluidics using picoinjectors. *Proc. Natl. Acad. Sci. U. S. A.* **107**, 19163-19166 (2010).
8. Frohnmayr, J.P. et al. Minimal Synthetic Cells to Study Integrin-Mediated Adhesion. *Angew. Chem.-Int. Edit.* **54**, 12472-12478 (2015).
9. Axelrod, D., Koppel, D.E., Schlessinger, J., Elson, E. & Webb, W.W. MOBILITY MEASUREMENT BY ANALYSIS OF FLUORESCENCE PHOTOBLEACHING RECOVERY KINETICS. *Biophys. J.* **16**, 1055-1069 (1976).
10. Soumpasis, D.M. THEORETICAL-ANALYSIS OF FLUORESCENCE PHOTOBLEACHING RECOVERY EXPERIMENTS. *Biophys. J.* **41**, 95-97 (1983).
11. Gracia, R.S., Bezlyepkina, N., Knorr, R.L., Lipowsky, R. & Dimova, R. Effect of cholesterol on the rigidity of saturated and unsaturated membranes: fluctuation and electrodeformation analysis of giant vesicles. *Soft Matter* **6**, 1472-1482 (2010).
12. Angelova, M.I. & Dimitrov, D.S. Liposome electroformation. *Faraday Discussions of the Chemical Society* **81**, 303-311 (1986).
13. Pott, T., Bouvrais, H. & Meleard, P. Giant unilamellar vesicle formation under physiologically relevant conditions. *Chemistry and Physics of Lipids* **154**, 115-119 (2008).
14. Weinberger, A. et al. Gel-Assisted Formation of Giant Unilamellar Vesicles. *Biophys. J.* **105**, 154-164 (2013).
15. Dimova, R. Recent developments in the field of bending rigidity measurements on membranes. *Adv. Colloid Interface Sci.* **208**, 225-234 (2014).
16. Nagle, J.F. & Tristram-Nagle, S. Structure of lipid bilayers. *Biochim. Biophys. Acta-Rev. Biomembr.* **1469**, 159-195 (2000).
17. Shattil, S.J., Kim, C. & Ginsberg, M.H. The final steps of integrin activation: the end game. *Nat. Rev. Mol. Cell Biol.* **11**, 288-300 (2010).
18. Cherney, D.P., Conboy, J.C. & Harris, J.M. Optical-trapping Raman microscopy detection of single unilamellar lipid vesicles. *Analytical Chemistry* **75**, 6621-6628 (2003).
19. Kim, H.S. et al. Raman spectroscopy compatible PDMS droplet microfluidic culture and analysis platform towards on-chip lipidomics. *Analyst* **142**, 1054-1060 (2017).